



Using a Gaussian Process Emulator to approximate the climate response patterns to greenhouse gas and aerosol forcings

Laura A. Mansfield^{1,2,3*}, Peer J. Nowack^{4,5,1}, Edmund M. Ryan⁶, Oliver Wild⁷, and Apostolos Voulgarakis^{1,8,9}

¹Department of Physics, Imperial College London, United Kingdom.

²School of Mathematics and Statistics, University of Reading, United Kingdom.

³Atmospheric, Oceanic and Planetary Physics, University of Oxford, United Kingdom.

⁴Climatic Research Unit, School of Environmental Sciences, University of East Anglia, United Kingdom.

⁵Institute of Theoretical Informatics and Institute of Meteorology and Climate Research (IMKASF), Karlsruhe Institute of Technology, Germany.

⁶AWE Aldermaston, Reading, Berkshire, UK

⁷Lancaster Environment Centre, Lancaster University, Lancaster, United Kingdom.

⁸Leverhulme Centre for Wildfires, Environment and Society, Imperial College London, United Kingdom.

⁹School of Chemical and Environmental Engineering, Technical University of Crete, Greece

Correspondence to: Laura A. Mansfield (laura.mansfield@physics.ox.ac.uk)

Abstract. We present a Gaussian process emulator for estimating fast surface temperature response patterns to a range of different climate forcing agents, including both long-lived greenhouse gases and short-lived pollutants such as aerosols. This emulator is trained on simulations driven by perturbations to emissions (for short-lived pollutants) and concentrations (for long-lived greenhouse gases) using a full-complexity global climate model and predicts the response in the first five years after the forcing, at a small fraction of the computational cost. We outline the emulator design, including the choice of pollutant perturbations and the input space covered by the training data. We show that the emulator performs well in most regions of the chosen input space, except under very large aerosol perturbations. A global sensitivity analysis is carried out to characterize and understand emission-response relationships for each pollutant. We find similar large-scale patterns of sensitivity to aerosol pollutants released in different regions. Finally, we demonstrate how this type of emulator could be used in policy-relevant studies to predict fast adjustments of regional climate to changes in anthropogenic emissions for a given scenario. This establishes a basis for rapid climate change projection, without the need for computationally expensive climate model simulations, and increases the number of climate change scenarios that can be explored simultaneously.

1 Introduction

Climate change projections are essential to inform society and policymakers about possible scenario-dependent impacts. To estimate the state of the future climate, we rely on Global Climate Models (GCMs) to run numerical simulations of the Earth system, including atmospheric, oceanic, land and sea-ice components and their interactions. These GCMs project the climate at a time in the future, given the current climate state and an emissions scenario that describes how the emissions/concentrations of greenhouse gases, aerosols and other atmospheric constituents are expected to evolve. Since future emissions are highly uncertain, GCMs must be run for a range of different possible scenarios. The output from a GCM can add to our understanding



of the individual and net effects of different anthropogenic forcings on the climate system, which has long been of interest to climate scientists. Furthermore, understanding the climate response to emissions can inform important policy decisions.

The high complexity and computational cost of climate and atmospheric modelling puts a limit on the number and range of climate projection studies that can be carried out. This has led to a recent increase in application of surrogate models that reproduce climate relevant variables given known inputs, at a much lower cost (Bolton & Zanna, 2019; Castruccio et al., 2014; Kaltenborn et al., 2023; Mansfield et al., 2020; Nowack et al., 2018; Rasp et al., 2018; Ryan et al., 2018; Watson-Parris, 2021; Wild et al., 2020). Here, we use a type of surrogate model called a *Gaussian process (GP) emulator*, which have become popular for aiding atmospheric and climate model development, through sensitivity analyses, uncertainty quantification and calibration (Carslaw et al., 2013; Lee et al., 2012; Ryan et al., 2018; Salter & Williamson, 2016; Williamson et al., 2015).

Climate model emulators are beginning to emerge with the primary aim of climate change projection. One approach currently gaining traction involves learning an *autoregressive model of the full climate state*, i.e., by predicting all climate variables at one timestep, given all climate variables at the previous timestep (e.g., Boussard et al., 2023; Cachay et al., 2024; Guan et al., 2024; Watt-Meyer et al., 2023, 2025). These require large-scale neural networks to capture all climate model variables and often suffer from instability when implemented over long timescales. These studies are also limited to only exploring a few forcings that have been included during training, such as through sea surface temperature forcing or CO₂ forcing (Watt-Meyer et al., 2025), and are yet to explore a wide range of climate change responses to different scenarios. In contrast, an alternative approach is to directly *learn the climate model response to a change in forcing*, often referred to as ‘reduced complexity models’ (Nicholls et al., 2020). This approach leverages simpler machine learning models to emulate the change in the climate state given a change in forcing, typically focusing on the response to different CO₂ scenarios (Bao et al., 2016; Castruccio et al., 2014; Foley et al., 2016). Most past emulation studies estimate the *global mean* response to forcings over a timeseries (Castruccio et al., 2014; Meinshausen et al., 2011; Smith, Forster, et al., 2018), with a few extending this to include spatial patterns (Bao et al., 2016; Beusch et al., 2022; Nath et al., 2022). The ability to predict climate response to changing forcings with quick, simple models is particularly valuable for policy-makers as they can be embedded within Integrated Assessment Models (IAMs, e.g., Foley et al., 2016) or can inform climate change scenario pathways (e.g., Durack et al., 2025; Forster et al., 2021).

In this paper, we present an emulator based on the HadGEM3 GCM. The emulator is designed to predict the temperature response patterns to a wide range of forcing types, including regional aerosol emissions and global greenhouse gas concentration changes. Specifically, the emulator predicts maps of the short-term global surface temperature response to different emission perturbations, i.e., the fast adjustment of the surface temperature, in the first 5-years following the perturbation. This fast adjustment emulator predicts the response to an abrupt change in emissions (such as the simulations run in idealized forcing-response studies, e.g., Myhre et al., 2017; Richardson et al., 2019; Stohl et al., 2015; Samset et al., 2018; Smith et al., 2018) and lays the foundations for the development of long-term climate response emulators and/or transient

emulators, for instance, through the coupling of multiple emulators designed to predict on different timescales (e.g., Mansfield et al., 2020). The emulator is designed to predict the entire spatial pattern of the global climate change response, rather than just the global mean, which could prove useful in future policy and impact studies.

75 In Section 2, we describe the emulator design including the choices of input variables and perturbation ranges. Section 3 considers the performance of the trained emulator on a set of test scenarios, on both regional and spatially resolved scales. In Section 4, the emulator is used to carry out a global sensitivity analysis to explore the main effects of each perturbation and the sensitivity of each region to local and remote emission perturbations. Section 5 shows a novel application of the emulator, where the short-term response is predicted for two Shared Socioeconomic Pathways (SSPs). Section 6 makes the concluding
 80 remarks on the study.

2 Emulator Design

85 2.1 Global Climate Model Configuration

The GP emulator is trained on simulations from the HadGEM3 model, in the third Global Coupled configuration 3.1 (GC3.1) (Williams et al., 2018) which consists of the global atmosphere-land (GA7/GL7.1) (Walters et al., 2019), global ocean (GO6) (Storkey et al., 2018) and sea-ice (GSI8.1) (Ridley et al., 2018). This configuration uses the modal version of the Global Model
 90 of Aerosol Processes (GLOMAP-mode), two-moment aerosol microphysics scheme (Mann et al., 2010). The model resolution is 1.25° latitude by 1.875° longitude, giving a grid cell of roughly 208 km by 139 km at the Equator. The same model configuration was employed for historical simulations in (Andrews et al., 2020), which formed part of the UK contribution to the sixth Coupled Model Intercomparison Project (CMIP6). 'Present-day' conditions are taken from the end of these simulations, and correspond to the year 2014. The present-day simulation was run for 300 years as 'spin-up', to reach an
 95 approximate equilibrium, and this was then used as the starting point for simulations that serve as training data for the emulator.

Before computing any perturbation runs, six 5-year-long control simulations were performed starting from this equilibrium state. To define the 'short term' surface temperature response, we take a temporal average over the 5 years of each control/perturbation simulation. All perturbation runs are initialized from the end of the long control run. The well-mixed
 100 GHGs are perturbed via their global concentrations, while for the short-lived pollutants we use scaling factors for emissions over broad regions, described further in Section 2.2. For each perturbation run, we define the surface temperature 'response' as the short-term surface temperature in the perturbation run minus the short-term surface temperature averaged across all six independent control runs. The surface temperature response is defined at every grid cell of the GCM, giving a complete spatial map.



105

2.2 Gaussian process emulator

The GCM provides us with surface temperature responses at all N grid cells, $\mathbf{y} = (y_1, y_2, \dots, y_N)$, given input values, \mathbf{x} , which describe the emissions scenario, i.e., we assume that the GCM gives

$$\mathbf{y} = f_{GCM}(\mathbf{x}).$$

110 We use a GP emulator to estimate the surface temperature response to a given emissions scenario, i.e.,

$$\mathbf{y}_{GP} = f_{GP}(\mathbf{x})$$

where $\mathbf{y}_{GP} \approx \mathbf{y}$. The GP emulator estimates the GCM response to different \mathbf{x} , although there is internal variability overlaying this (i.e., noise), which makes weaker responses more difficult to predict. While we do not attempt to model this noise explicitly, we take advantage of the GP emulator's ability to estimate uncertainty about the prediction and assume that a portion
 115 of this uncertainty is due to the internal variability of the GCM. Note that \mathbf{y} and \mathbf{y}_{GP} are vectors containing the estimated surface temperature response at each grid cell. Here, we build separate GP emulators for each grid cell. We learn the function, f_{GP} , by training the GP emulator with input-output pairs (\mathbf{x}, \mathbf{y}) obtained from GCM simulations. In the following section, we describe how input values were chosen, including the choice of pollutants that are varied and the range of possible values they can take.

120

2.3 Choice of inputs and ranges

Due to the high cost of running the GCM, we aim to minimize the number of simulations required to build and test this
 125 emulator. This can be done with a careful choice of inputs and a space-filling design of these inputs (Currin et al., 1991). First, we limit the number of possible inputs to the dominant climate forcings. These include well-mixed climate pollutants, specifically the two most important anthropogenic greenhouse gases carbon dioxide (CO_2) and methane (CH_4) (Stocker, 2013). For the short-lived pollutants, we perturb sulfur dioxide (SO_2 , the precursor to sulfate aerosol (SO_4)) and biomass burning (BB) carbonaceous aerosols (black carbon (BC) and organic carbon (OC)). Sulfate aerosol is chosen because it has a strong
 130 cooling impact on the climate, particularly at a regional level, and because its precursor is emitted mostly from fossil fuel burning, making it highly relevant for scenario projection studies (Stocker, 2013). BB OC/BC are chosen as they strongly affect the climate through scattering and absorption of radiation and due to their dominance in the tropics (Boucher et al., 2013; Haywood & Boucher, 2000). In addition, BB is a particularly high source of scenario uncertainty, but has not been studied as extensively as other forcing perturbations (Lasslop et al., 2019; Tosca et al., 2013; Voulgarakis & Field, 2015; Ward et al.,
 135 2012). While other pollutants (e.g., NO_x , NMVOCs, OC/BC from other sources) are also relevant for climate change, we keep these fixed at present-day levels because even for large perturbations, the effects are too small to exceed the regional climate noise in any of our simulations and thus are less useful for training the emulator (Aamaas et al., 2019; Baker et al., 2015; ECLIPSE, 2014; D. Shindell & Faluvegi, 2009; Stohl et al., 2015).



140 For the greenhouse gases, we apply global perturbations to their concentrations in the GCM as they have long lifetimes and relatively homogeneous spatial forcing. For the short-lived pollutants, we perturb the emissions fields for the GCM. As the region of emission is paramount when considering the effect of short-lived pollutants, these perturbations are made over regional scales. We select broad continental regions in which short-lived emissions are scaled up or down (e.g., 2x, 0.5x), while keeping the spatial distribution of emissions within each region unchanged.

145 Following the procedure used in previous studies, we perturb SO₂ in North America, Europe, East Asia and South Asia (the same regions as (Kasoar et al., 2018; Lewinschal et al., 2019; Westervelt et al., 2020)), by scaling the regional present-day distribution of emissions. This approach allows for the entire region to be represented by a single scaling factor, but restricts the emulator to scenarios where the spatial distribution of emissions within each region does not change significantly. In other words, it does not account for the possibility of new emission hotspots within each region. This assumption is made because in these four regions, SO₂ emissions are predicted to decline in the future (Westervelt et al., 2020, Lund et al., 2019).

We further extend our study by perturbing SO₂ in Africa and South America, which currently have low levels of SO₂ relative to the rest of the world but are likely to see increasing emissions in the coming decades, due to changes in land use and industrialization in South America (Popp et al., 2017) and rapid growth of cities in Africa (Lioussé et al., 2014). For these regions, the assumption of a constant spatial distribution of emissions may not be valid, as present day SO₂ emissions are low and originate from isolated hotspots (see Supplementary Fig. S1). We therefore use the emission distribution from the SSP5 baseline scenario with rapid growth (Riahi et al., 2017) to represent future conditions, while keeping total emissions fixed. (Supplementary Fig. S1).

160 Finally, we perturb BB OC/BC in the tropics (between 24 °S and 24 °N), which covers tropical regions of Africa, South America and South East Asia, where biomass burning due to fires is the largest source of OC/BC (Cachier et al., 1989; Pechony & Shindell, 2010; Tosca et al., 2013; Van der Werf et al., 2003). We perturb OC and BC in the same proportions, assuming that their ratio remains constant, following other studies (Hodnebrog et al., 2016; Tosca et al., 2013). This allows the emulator to be used to explore future scenarios under different levels of tropical biomass burning, whether it be due to anthropogenic suppression/ignition, a consequence of a warmer planet (e.g., alongside increasing GHGs) or under natural variability (Pechony & Shindell, 2010). We do not consider OC/BC on smaller regional scales because previous studies find that large, unrealistic OC/BC forcings are required to obtain a climate response that exceeds the internal climate noise (e.g., Myhre et al., 2017; Baker et al., 2015; Stohl et al., 2015).

170 This gives a total of nine inputs, two of which are the global GHG concentrations and seven of which are regional scaling factors of short-lived pollutant emissions, as shown in Table 1. For each input, we define an input space that encompasses the



range of possible scenarios of interest to policy-makers and climate scientists, based on the minimum and maximum plausible values estimated by previous studies, which include projections of the Shared Socioeconomic Pathways (SSPs) (Riahi et al., 2017; van Vuuren et al., 2017) and Evaluating the Climate and air quality Impacts of short-lived pollutants (ECLIPSE) project (Aamaas et al., 2017; Baker et al. 2015; ECLIPSE, 2014; Stohl et al., 2015), as well as other individual studies (Lioussé et al., 2014; Pechony & Shindell, 2010). For the greenhouse gases, we take the pre-industrial levels as the minimum value and for the short-lived pollutants we take the minimum value as a scaling factor of zero, representing near-idealized anthropogenic pollution-free conditions. For all forcings, we determined the maximum levels to be the worst-case estimate from both future projections and historical scenarios (up to pre-industrial) in previous studies. Table 1 shows the ranges selected for each input and the reasoning behind the maximum values. Note that these 'maximum' scaling factors do not reflect realistic scenarios, but are chosen as an appropriate upper limit for scenarios that one may wish to emulate.

The fact that we apply regional perturbations to the short-lived pollutants inevitably leads to small changes in abundances and weak forcings. This can give weaker grid-scale climate response signals that are difficult to separate from the internal noise (Kasoar et al., 2018; Shawki et al., 2018). For this reason, we extend the input space beyond the ranges described in Table 1 for these forcings, in order to create an emulator that gives less uncertain results. We expect that including simulations with stronger perturbations, which should have larger signal-to-noise ratios, could be beneficial for constraining the emulator prediction to these perturbations. We therefore extend the input space for the short-lived pollutants only so that 75% of simulations fall within the input range indicated in Table 1 and the remaining 25% lie outside this but within a range that is double this (see Supplementary Fig. S2). This makes our emulator more capable of capturing responses to large idealized perturbations in short-lived pollutants, which are common in scientific studies exploring the physical processes linking short-lived pollutant forcing and response (Liu et al., 2018; Myhre et al., 2017; Richardson et al., 2019).

195



Table 1. All input and the ranges used in the emulator, with associated reasoning for maximum value. The minimum values are taken to be pre-industrial concentrations for CO₂ and CH₄ and a scaling factor of zero for all short-lived pollutants.

Input	Range	Reasoning
Global CO ₂ concentration	282 - 834 ppm	SSP3 baseline projection in 2100 (Riahi et al., 2017)
Global CH ₄ concentration	248 - 3238 ppb	SSP3 baseline projection in 2100 (Riahi et al., 2017)
SO ₂ over North America	0 – 3x	Historical data from 1990 (ECLIPSE, 2014)
SO ₂ over Europe	0 – 5x	Historical data from 1990 (ECLIPSE, 2014)
SO ₂ over East Asia	0 – 2x	Historical data from 2005 (ECLIPSE, 2014) and SSP1 projection in 2100 (Riahi et al., 2017)
SO ₂ over South Asia	0 – 3x	ECLIPSE projection in 2030 (ECLIPSE, 2014)
SO ₂ over Africa	0 – 7x	Inventory based projection in 2030 (Lioussé et al., 2014)
SO ₂ over South America	0 – 3x	SSP3 baseline projection in 2080 (Riahi et al., 2017)
BB OC/BC over Tropics	0 – 2x	Estimates of fire activity by 2100 (Pechony & Shindell, 2010)

200

2.4 Design of training data

We design a set of training simulations by selecting combinations of input values that will be inputs to the GCM. The best approach to do this is to generate sets of input values that are space-filling (e.g., Currin et al., 1991; Lee et al., 2016; O’Hagan, 1978; Ryan et al., 2018; Santner et al., 2003; Wild et al., 2020). This minimizes the number of samples needed to cover the input space efficiently, which is particularly important for this study as model simulations are computationally expensive (around 80 node hours per simulation on a Cray XC40 (Met Office, 2021)). An informal rule of thumb is that the number of runs for training should be around 10 times the number of input dimensions (Loeppky et al., 2009), and this approach has worked well in previous climate model emulators (e.g., Carslaw et al., 2013; Lee et al., 2012; Ryan et al., 2018). Given the nine inputs of interest in this study and the high computational cost of the simulations, we perform 80 simulations for training. These 80 training points are selected to be space-filling by using a Latin Hypercube Sampler (LHS), which subdivides the input space evenly and samples each partition so that the distance between samples is maximized (e.g., Lee et al., 2011, 2012; Ryan et al., 2018). The samples are shown in Supplementary Fig. S2. We also perform an additional 18 simulations for testing, which are sampled separately from the ranges in Table 1 using an LHS design.

215

2.5 Gaussian process emulator details



With the 80 training simulations available, we build an emulator to project the short-term surface temperature response based on the nine inputs that control the CO₂ and CH₄ concentrations and the short-lived emission scaling factors described above (Table 1). Prior to building the emulator, the inputs and outputs are scaled to be centered around 0 with standard deviation of 1. Separate GP emulators are then applied to estimate the surface temperature response for each grid-cell independently. For each grid cell, the GP emulator is

$$f_{GP}(\mathbf{x}) = \mathcal{G}(m(\mathbf{x}), K(\mathbf{x}, \mathbf{x}'))$$

where $m(\mathbf{x})$ is the prior mean function and $K(\mathbf{x}, \mathbf{x}')$ is the prior covariance function or “kernel” that describes the covariance between two inputs, \mathbf{x} and \mathbf{x}' . The choice of $m(\mathbf{x})$ and $K(\mathbf{x}, \mathbf{x}')$ controls the structure of the GP emulator (Rasmussen & Williams, 2006). The prior mean function is often assumed to be zero so that all choices are determined by the covariance function, as done here. The kernel defines the similarity of two inputs \mathbf{x} and \mathbf{x}' and how this propagates through to the similarity of the outputs $\mathcal{G}(\mathbf{x})$ and $\mathcal{G}(\mathbf{x}')$. For this, we use an additive kernel consisting of a linear kernel, a squared exponential kernel and a white noise kernel, where the latter represents the internal variability of the GCM, assumed to be constant for all predictions (described below). We found the emulator to be robust to a range of kernel choices (Supplementary Fig. S3). We learn the hyperparameters of the linear and squared exponential kernels through maximum likelihood estimation, using the python library, GPy (GPy, 2012). We also tested different methods such as random forests but we did not find improvements in performance, so we focus only on GP emulators here.

In this study, we consider two types of uncertainty. Firstly, we view the uncertainty associated with the chaotic nature of the Earth system, the aleatoric uncertainty (Shepherd, et al., 2018), as a limitation of the GCM prediction, and secondly, we diagnose the uncertainty due to the emulator prediction being an approximation of the GCM at new unseen scenarios not within the training set (which we call the predictive uncertainty). As a GP emulator is a Bayesian method and predicts a distribution of responses, the latter is a natural output of each prediction. Note that we do not consider the uncertainty caused by the difference in the GCM predictions and the truth, i.e., epistemic uncertainty or model inadequacy/discrepancy.

The uncertainty due the chaotic nature of the GCM is the internal variability, σ_{GCM} , and is estimated as the standard deviation between as many 5-year control runs as available. We have available 8 segments from one long, 40-year control run after equilibrium had been reached in the spin-up simulation, and 6 independent 5-year control runs that branched off from this. Ideally, all control runs would be strictly independent but the 8 segments of the longer control run are included to improve the sample size for estimating the standard deviation. The standard deviation across the 14 control runs is calculated for each grid point independently, giving a map of uncertainty associated with the internal noise. This is an uncertainty associated with any prediction from the GCM, and is partly due to the limited number of years we have averaged over. We expect this to be present for any prediction and therefore, we include this as a fixed noise term in our emulator, implemented as a white noise covariance function of the GP emulator. When the emulator predicts the temperature response at new unseen input values, there is also predictive uncertainty provided by the GP emulator, which we label σ_{GP} . The total uncertainty arising from both the GCM



internal variability and the GP emulator prediction is denoted σ_{total} and these are related via $\sigma_{\text{total}}^2 = \sigma_{\text{GCM}}^2 + \sigma_{\text{GP}}^2$, discussed later in Section 3.3.

255

3 Emulator Performance

To test the performance of the emulator, we predict the output for 18 test simulations that have not been used for emulator training, where the input values have been generated with a Latin Hypercube Sampler, with a uniform distribution across all input ranges of interest (Table 1).

260

3.1 Global response predictions

Figure 1 shows an example of typical emulator performance, with the input values shown along the top panel, relative to the baseline, minimum and maximum possible values. The maps show, from top to bottom, the GCM output for the test scenario, y_{test} , the GP prediction, y_{pred} , and the absolute errors, $|y_{\text{pred}} - y_{\text{test}}|$, with the stippling indicating regions where this exceeds 1 s.d. predicted by the GP emulator. This example is representative of the test simulations which are presented in Supplementary Fig. S4. Most test simulations are reasonably well predicted by the emulator and show patterns of warming or cooling generally in the correct spatial location, similar to **Figure 1** (see Supplementary Fig. S4 for all scenarios). The absolute difference is generally larger at high latitudes, particularly around the Arctic, Greenland and Northern Europe. Although the magnitude of σ_{total} is slightly larger in these regions than in the tropics, the stippling where $|y_{\text{pred}} - y_{\text{test}}| > \sigma_{\text{total}}$ is more prominent in these high latitude areas, indicating that prediction is poorer there compared to other regions worldwide. These regions are highly correlated with the regions that experienced larger errors in our previous emulation study that found these to be areas that experience both increased sensitivity to forcings and increased variability (Mansfield et al., 2020). Statistically, we would expect ~32% of predicted points to fall outside the 1σ prediction level, which is generally the case across all test scenarios, with the exception of Supplementary Fig. S4k. However, the predicted points that fall outside this accuracy threshold have a specific regional pattern and occur more often in the Northern Hemisphere, rather than being distributed randomly across the globe.

270

275

For the test scenario in Supplementary Fig. S4k, the emulator predicts the correct sign of response in most regions, but the prediction is too weak in magnitude compared to the GCM. We believe this to be because the inputs are all strongly positive relative to present-day levels meaning this scenario falls close to the corner of the input space, where there are fewer training data points to constrain the prediction. The emulator overestimates the cooling effect of strong aerosol perturbations, highlighting that caution should be taken when interpreting emulator predictions on very strong aerosol perturbation scenarios.

280



285 Future studies may wish to refine the accuracy of the emulator in this region of the input space, by running additional training
simulations with even stronger aerosol perturbations. The remainder of this study does not focus on the strong aerosol
perturbation regime since we consider more realistic emission perturbations. Overall, however, the test simulations indicate
that the GP emulator can predict the response to a range of scenarios under these nine inputs. Based on all 18 test simulations,
76.1% of grid points are predicted to within 1σ of the true response and 95.0% are predicted to within 2σ , which is roughly
290 in line with expectations, assuming a Gaussian distribution of responses.



295

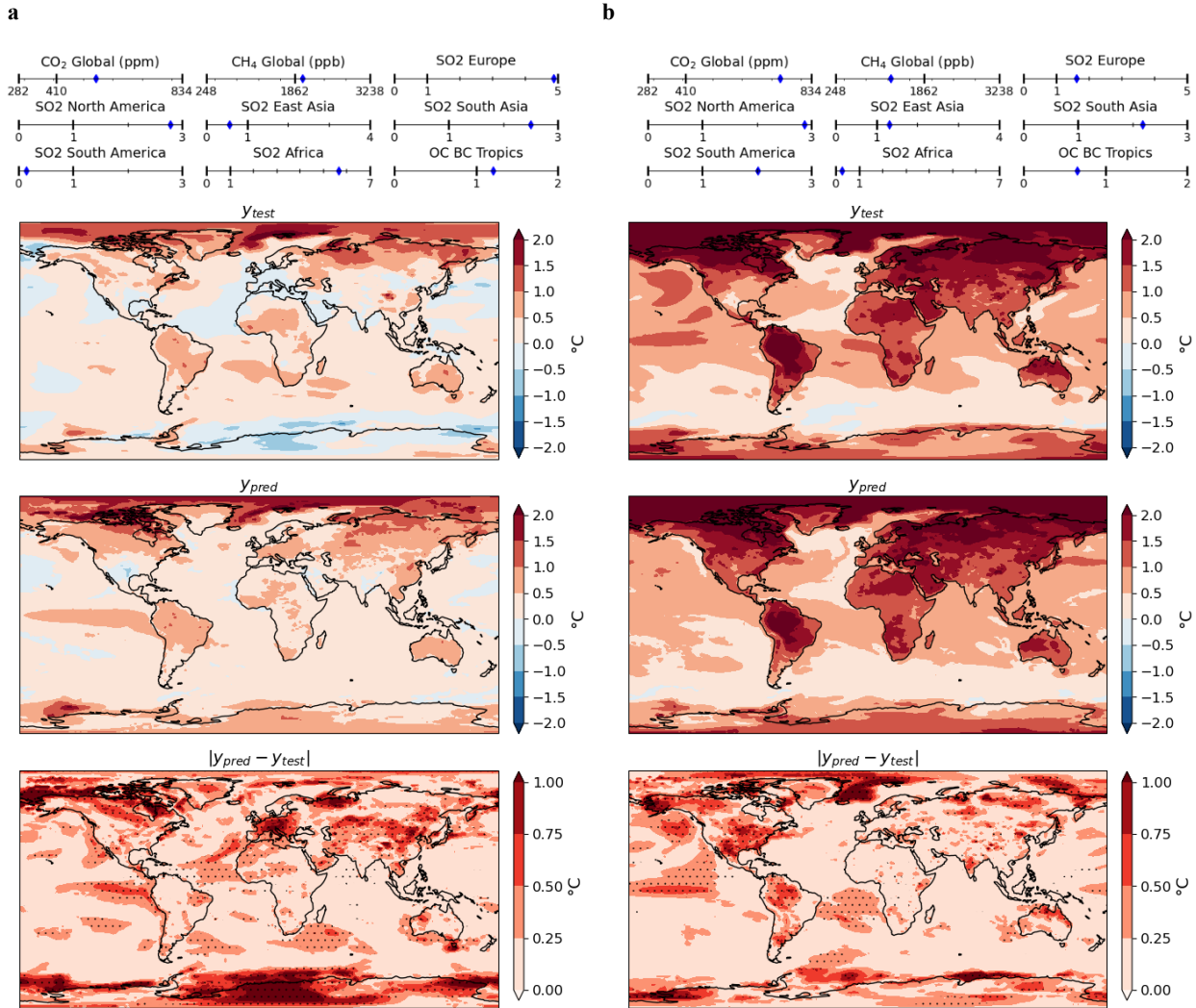


Figure 1. Two example test scenarios, where top panel shows inputs values, as well as the baseline, minimum and maximum possible values. The maps show, from top to bottom, the GCM output for the test scenario, y_{test} the GP prediction, y_{pred} and the absolute errors, $|y_{pred} - y_{test}|$, where in the latter the stippling indicates regions where this absolute error exceeds 1 s.d. predicted by the GP emulator, $|y_{pred} - y_{test}| > \sigma_{total}$.

3.2 Regional mean response predictions



We have also assessed the response for each region by taking broad averages over areas of interest. The response predicted by the GP emulator is plotted against the true GCM response for all test scenarios in Figure 2 where the error bars indicate the 1σ uncertainty levels. A perfect prediction would correspond to the $y = x$ line (black dashed line), a coefficient of determination $R^2 = 1$ and a mean absolute difference (MAD) equal to zero. Most regional mean predictions fall very close to this line, or within 1σ from it. The exception to this is the outlier with a positive true response of around 1°C in most regions, that is strongly underestimated, which corresponds to the test scenario in Supplementary Fig. S4k. Other than this scenario, the majority of responses are well predicted and cover a fairly broad range of responses including both cooling and warming of up to $1\text{--}2^\circ\text{C}$ (R^2 values are all above 0.87). These plots also highlight the increased uncertainty associated with some regions, namely North America and Europe, in comparison to the tropical regions such as South Asia, South America and Africa. As well as exhibiting increased uncertainties, these regions also show a wider range of temperature responses in the test data. This leads to slightly higher absolute errors (increased MAD values) in these regions, but overall each prediction is still close to the ground truth (GCM), as highlighted by the high R^2 values. This gives confidence to the use of an emulator in this way for quick predictions, for instance in policy-relevant studies.

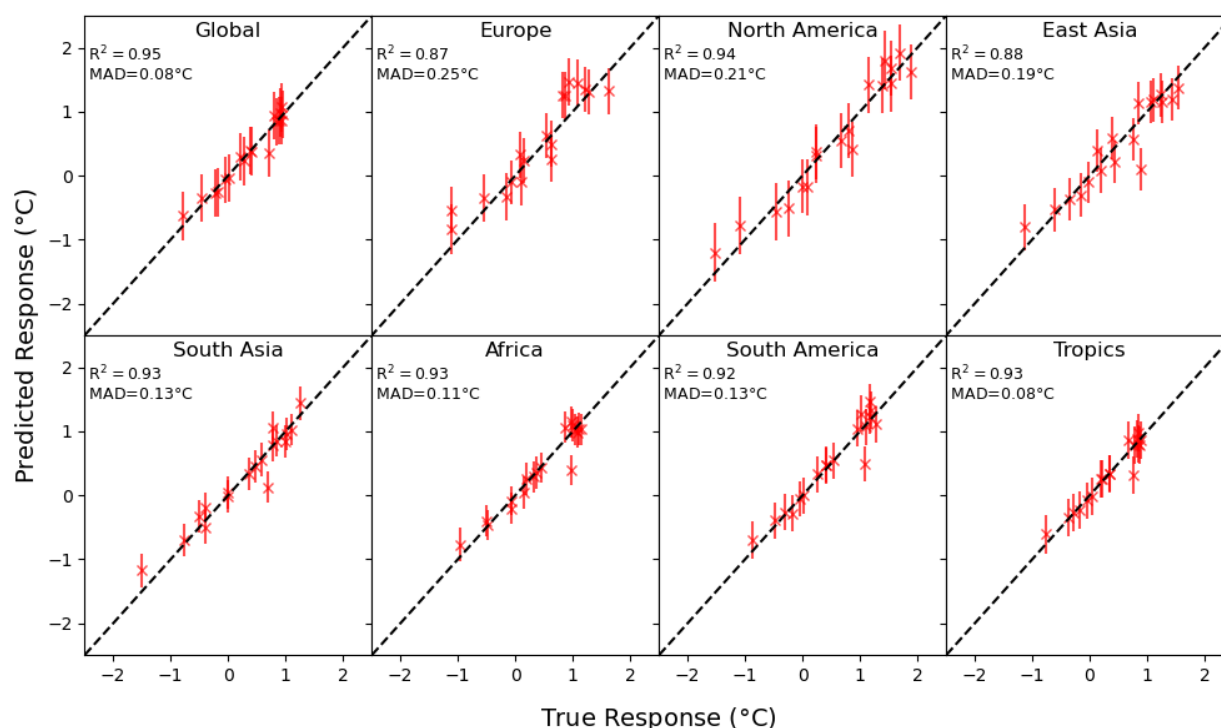




Figure 2. Regional mean predicted responses of test simulations against true GCM response, where error bars represent 1σ uncertainty level of Gaussian process prediction, for the main regions of interest, including the global mean. The coefficient of determination R^2 and the mean absolute difference (MAD) is also shown for each region.

325 3.3 Internal variability

We used the internal variability of the GCM as a fixed component of uncertainty when building the emulator, in order to view it as a form of aleatoric uncertainty, in other words, caused by the unpredictability of the system and intrinsic to any GCM prediction. The internal variability is calculated over 14 control simulations of 5-year segments, and is shown in Supplementary Fig. S5a. The GP emulator provides an additional predictive uncertainty when predicting new scenarios, but this uncertainty is generally much smaller than the internal variability (Supplementary Fig. S5b). For comparison, we built versions of GP emulators without including a fixed contribution to the uncertainty from the internal variability. This emulator performs virtually identically and reproduces almost exactly the same distribution of total uncertainty (Supplementary Fig. S5c,d). This result is encouraging, as it suggests that even without providing the GCM internal variability, the GP emulator is able to learn it as a form of uncertainty. This suggests that the accuracy of the emulator is limited primarily by GCM internal variability when predicting the short-term surface temperature response.

4 Global Sensitivity Analysis

The climate modelling community has benefited from a wide range of GP emulation studies concerned with uncertainty quantification and sensitivity analysis, which aim to characterize the uncertainty on the outputs and identify where it arises from. Due to the high computational cost of GCM simulations, GP emulators have been utilized to diagnose uncertainties and sensitivities in a wide range of GCM components and settings, including atmospheric chemistry models (Beddows et al., 2017; Lee et al., 2012; Stell et al., 2021; Wild et al., 2020), sea-ice models (Edwards et al., 2019; Urrego-Blanco et al., 2016), climate-vegetation models (Bounceur et al., 2015), convection parameterizations (Souza et al., 2020), and atmospheric gravity waves (King et al., 2024). The inputs to these are typically climate model parameters that are not known perfectly, where gaining an understanding of how sensitive the outputs are to each input parameter is beneficial for model development and calibration. In this study, the inputs are emission perturbations and we are primarily interested in exploring patterns of potential future climate responses to a range of scenarios. Sensitivity analysis can be used to deepen our understanding of the sensitivity of climate across all world regions to different competing emissions. In particular, we carry out a global sensitivity analysis, which quantifies sensitivities to each input averaging over the effects of all other inputs (Saltelli et al., 2019; Saltelli & Annoni, 2010).

4.1 Main Effects



355 Firstly, we explore the “main effect” of each pollutant, meaning the effect of each pollutant on the output independent of all
 other pollutants. This is done by using the emulator to predict surface temperatures across the full range of possible input
 values for the pollutant of interest, while randomly sampling all other inputs repeatedly. This generates a set of many
 independent realizations, where here we use 200 realizations for our sensitivity analysis. We average over all realizations to
 find the main effect attributed to the pollutant of interest. Here, we wish to assess the main effect of the pollutants relative to
 360 the present-day climate and therefore we sample all other inputs from a normal distribution, centered at present day levels.

The mean behavior of each pollutant perturbation is calculated by averaging over the 200 different realizations and can be
 found in Supplementary Fig. S6 for each key region. The main effects of CO₂ are much stronger in all regions than the other
 pollutants. As expected, local aerosol perturbations give rise to stronger responses in the region of emission (particularly SO₂
 365 released over Europe, East Asia and South Asia), and often the second most important contributor is an emission perturbation
 in an area that is closer to the area examined than others (e.g., Africa is sensitive to SO₂ from Europe, also noted in Dong et
 al., 2014) South Asia is influenced by East Asia, also see Shawki et al., 2018). Additionally, remote regions show reduced
 response, often near zero. We find that the main effect is approximately linear for all pollutants, both GHGs and aerosols, over
 the ranges explored here, which is intuitive under small forcing perturbations (Boer & Yu, 2003; Gregory et al., 2004; Hansen
 370 et al., 1997); (Collins et al., 2013; Hansen et al., 2005; Richardson et al., 2019). However, we would expect to see non-
 linearities in the response when extending to larger forcing perturbations due to the saturation of aerosol-cloud interactions
 (Carslaw et al., 2013; Kasoar et al., 2018), as discussed further in Supplementary Text S1. This likely explains the
 overestimation of cooling due to strong aerosol perturbations in test scenario in Supplementary Fig. S4k.

375 Figure 3 summarizes the main effect per unit Tg of emissions for the aerosol perturbations, in each emission region, estimated
 as the gradients in the main effects plots (Supplementary Fig. S6), with the error bars representing the 1 s.d. uncertainty
 propagated from the main effects. These demonstrate similar patterns to previous studies that explore the temperature change
 per unit Tg emissions, following an abrupt emission perturbation (Aamaas et al., 2017; Collins et al., 2013; Shindell &
 Faluvegi, 2009). For instance, both Aamaas et al. (2017) and Kasoar et al., (2018) find European SO₂ perturbations to
 380 consistently produce larger responses per unit Tg than East Asian SO₂. (Shindell & Faluvegi, 2009) also find that broad
 latitudinal SO₂ perturbations in the tropics give fairly similar responses globally, while Northern hemispheric perturbations
 responses are much stronger in the latitude band of emission relative to other regions. Figure 3 shows consistencies with this
 as the Northern hemispheric perturbations show much stronger regional effects in other Northern hemispheric response regions
 while tropical perturbations (SO₂ Africa, South Asia, and South America) show more evenly distributed responses after
 385 accounting for the localized effect. Note that here we focus only on the 5-year response, rather than 20 years or longer explored
 in other studies and also that we average over the effect of other pollutants, in contrast to previous studies that keep them fixed
 at present-day levels based on simulations where one pollutant at a time is varied (Aamaas et al., 2017; Collins et al., 2013;
 Shindell & Faluvegi, 2009). This is also one of the first studies to explore the response to regional tropical perturbations (SO₂

South America, SO₂ Africa and OC/BC Tropics) as well as extratropical (e.g., Persad & Caldeira, 2018; Westervelt et al.,
 2020), rather than broad latitudinal perturbations (e.g., Aamaas et al., 2017; Collins et al., 2013; Joshi et al., 2003; Shindell &
 Faluvegi, 2009; D. T. Shindell, 2012). The main effects of the OC/BC tropical perturbation show more diversity between
 regions. There are local decreases in temperature over Africa, where the majority of the BB emissions are released. This is
 because, although the absorbing effect of BC aerosol increases temperatures globally (e.g., North America, South Asia), it
 reduces incident radiation to the surface, which is combined with the cooling effect of scattering from OC (Wells et al., 2022).

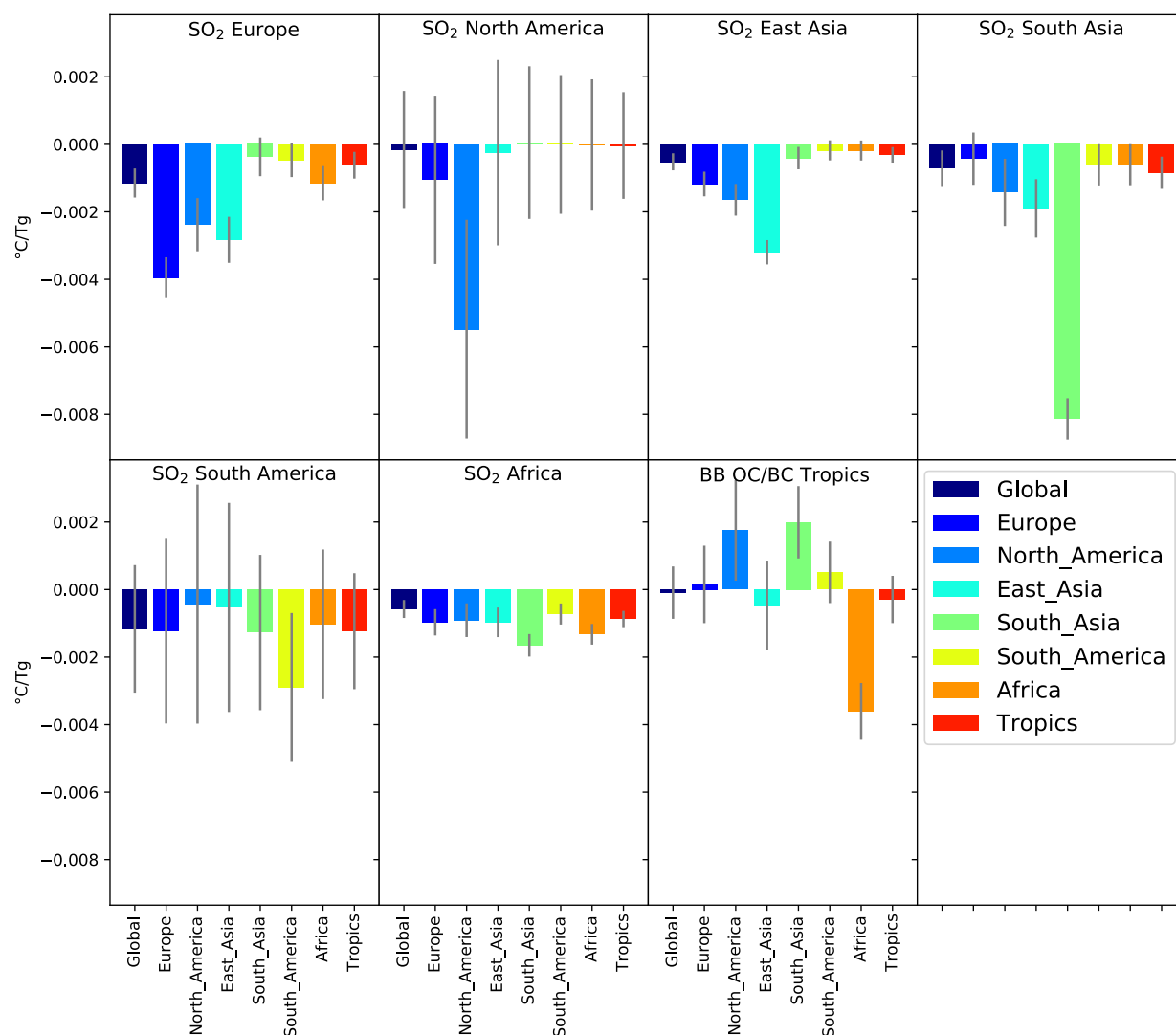


Figure 3. The expected change in temperature ($^{\circ}\text{C}$) for every 1 Tg increase of each aerosol pollutant in each response region. The values are estimated from the gradients of the lines of each plot in Supplementary Fig. S6, based on the linear relationships



found between the response in °C and the aerosol emission perturbation. The error bars represent 1σ uncertainty estimated by
 400 200 different realizations.

4.2 Sensitivity Indices

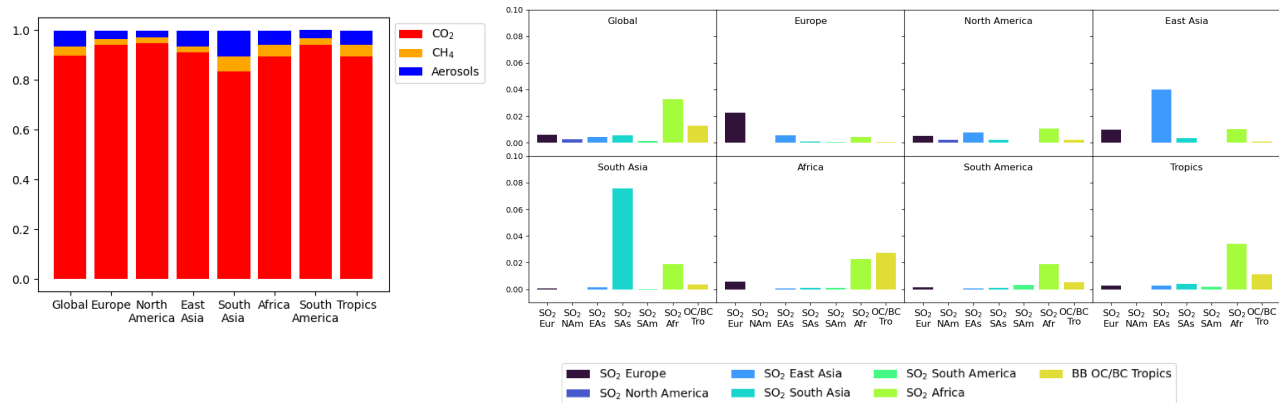
We have also carried out a variance-based global sensitivity analysis, by estimating how much of the variance in the output
 405 can be attributed to the variance in the inputs via the Sobol method (Saltelli et al., 2008, 2010). This can be calculated for each
 output variable at each grid point. Figure 4a shows the global and regional means of first order sensitivity indices for CO₂,
 CH₄ and aerosols, with a more detailed breakdown for each aerosol pollutant in Figure 4b. Firstly, the variance due to the CO₂
 concentration is responsible for the majority of the variance in the emulator (~90%) across all regions, which is not surprising
 given the wide input ranges covered by the emulator based on the high uncertainty of future CO₂ emissions. The first order
 410 sensitivity indices to CO₂, CH₄ and the aerosols sum to one almost exactly, leaving $< 10^{-4}$ down to higher order terms, indicating
 that there are only relatively weak interactions between the effects of the different inputs, described further in Supplementary
 Text S2. Figure 5 shows the sensitivity analyses for each grid-point, highlighting a fairly homogeneous spatial response for
 the greenhouse gases, but inhomogeneous spatial responses for the aerosol pollutants. Aside from the strong localized effect,
 the patterns of sensitivity to SO₂ from Europe and East Asia are remarkably similar; reminiscent of results from Kasoar et al.
 415 (2018), where removal of SO₂ from different Northern Hemisphere regions gave similar temperature response patterns.
 Additionally, the perturbations in tropical regions (SO₂ from South America, Africa and South Asia and OC/BC from the
 Tropics) give rise to similar distributions of sensitivity indices, with enhanced sensitivity over the tropical Atlantic and Pacific
 oceans. This mirrors the enhanced temperature sensitivities over the Northern hemispheric oceans due to the Northern
 hemispheric perturbations, an indication that the climate response is projected onto existing modes, in line with previous
 420 studies (Corti et al., 1999; Kasoar et al., 2018; Palmer, 1999; Ring & Plumb, 2008; Shindell et al., 1999).

425

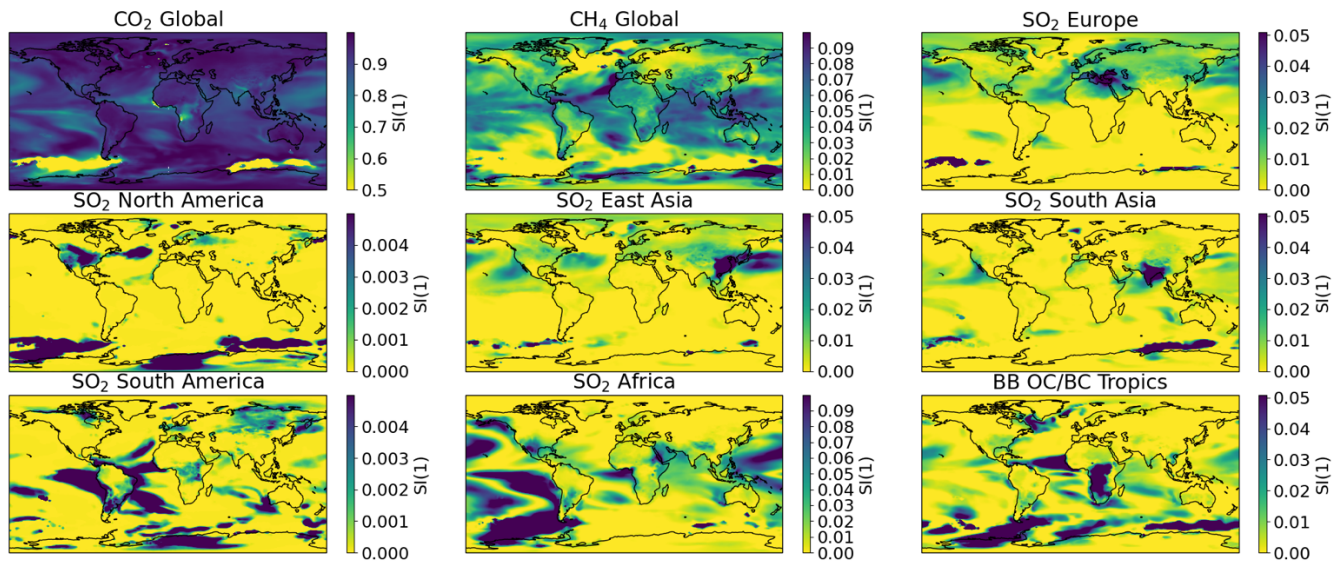
430

a

b



435 **Figure 4.** Regional mean first order sensitivity indices a) for CO₂, CH₄ and all aerosols in each region and b) breakdown of the aerosol sensitivity indices: the regional SO₂ perturbations and the tropical biomass burning aerosols (OC/BC).



440

Figure 5. Global maps of first order sensitivity indices, SI(1), for each pollutant perturbation to emulator, where SI(1) is the fraction of contribution to the total sensitivity for each pollutant. Note the different color bar ranges on each subfigure.

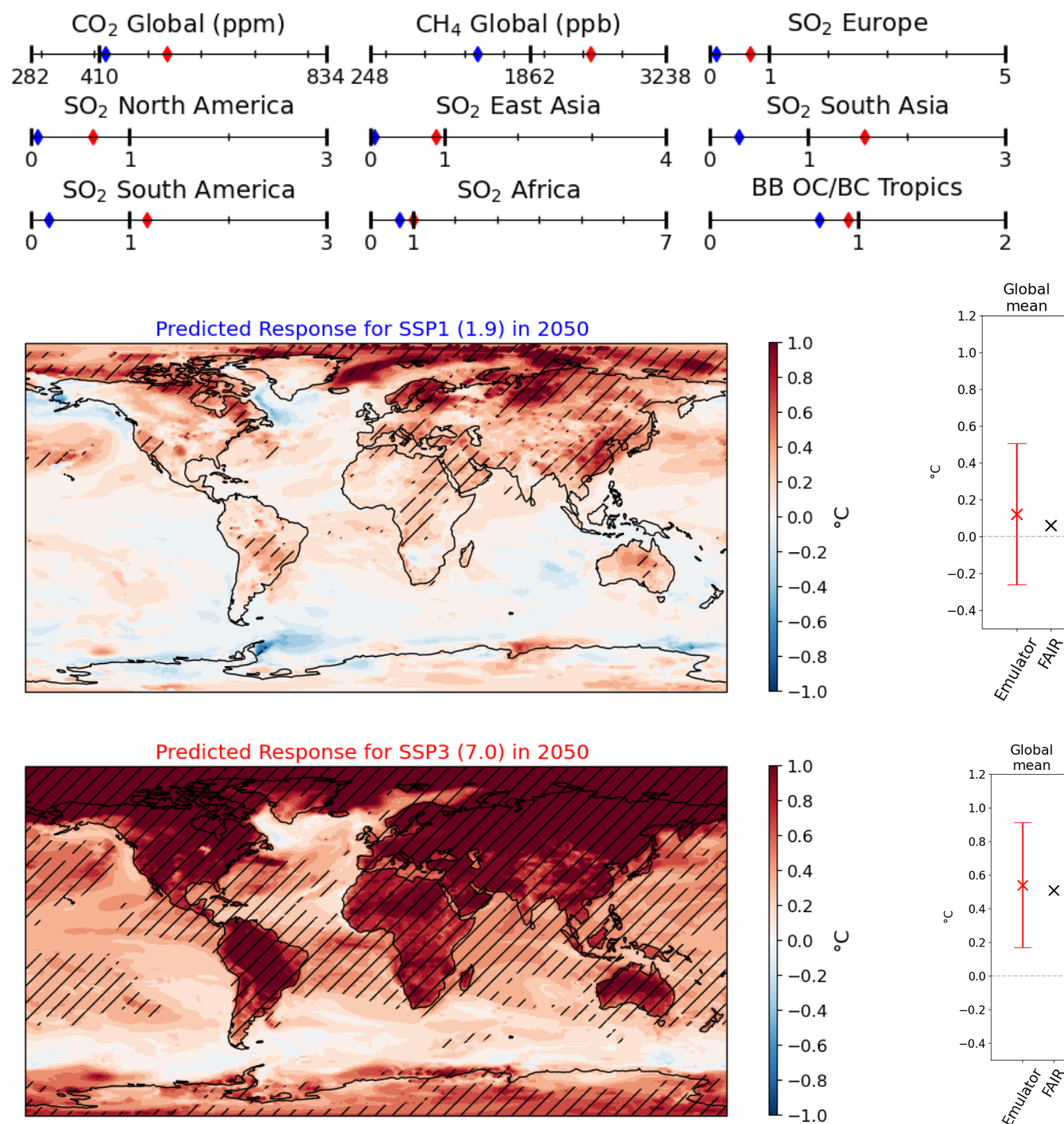
445 **5 Emulator Application**



The emulator developed in this study has been shown to successfully predict the responses to a range of GHG and aerosol perturbations, especially for realistic aerosol perturbations. In this section, we now explore how the emulator could be used to estimate the response to mid-century (2050) conditions from the Shared Socioeconomic Pathways (SSPs), which project socio-economic changes and their associated emissions into the future. We compare the emulator prediction for two contrasting scenarios: SSP1-1.9, the most optimistic low emissions scenario in line with Paris Agreement targets, and SSP3-7.0, a medium-high emissions scenario where countries focus on domestic development (Riahi et al., 2017).

These two scenarios project vastly different GHG and aerosol perturbations, with SSP1-1.9 projecting reductions in both GHG and aerosol emissions, which leads to stabilized CO₂ concentrations, reduced CH₄ concentrations and very low levels of SO₂ emissions by the end of the century in all regions (Meinshausen et al., 2020). In contrast, SSP3-7.0 projects a steady increase in GHG concentrations and a divergence in SO₂ emissions across the differing regions. A time slice of the 2050 GHG concentrations and aerosol emissions is taken to predict the response to the pollutants that the emulator considers (CO₂, CH₄, regional SO₂ and tropical biomass burning, which contribute to around 80% of the total forcing (Gidden et al., 2019)). These inputs are shown in the top panel of Fig. 6, alongside the response maps, where again the stippling indicates where the response exceeds the 1 σ level predicted by the emulator (i.e., the emulator is confident of the sign of response to at least 1 σ). For SSP1-1.9 there is a rise in surface temperature, predominantly in the Northern Hemisphere and over land, due to the decreases in SO₂. In the SSP3-7.0 scenario, the dramatic increase in GHG concentrations dominates the prediction, with large increases in surface temperature everywhere, which is again much stronger over land (Cubasch et al. 2001; Sutton et al., 2007).

Note that this emulator does not predict the transient response to the SSP scenarios between present day and 2050, but rather it estimates the short-term climate response to an abrupt jump in emissions and concentrations, from present-day to 2050 projected levels. We refer to this as a 'fast adjustment' emulator. Supplementary Fig. S7 shows the global mean response of the fast adjustment emulator compared to the predicted global mean of the same conditions using the FAIR model, a simple impulse response model that estimates the global mean response to changing emissions/concentrations (Smith et al., 2018). Both the emulator and FAIR models give almost identical estimates of the fast adjustment (right hand panel, Fig. 6), but this differs significantly from the response expected by a transient model, such as the CMIP6 estimates (see, e.g., Tebaldi et al., 2021). For many policy-related studies, the transient response is of interest, which requires further work to account for a full time series of emissions scenarios. However, to gain insight into the effect of a particular emission scenario under the 'idealized' setting, this fast adjustment emulator is a useful first step. This could be combined with another independently trained emulator that estimates the long-term (quasi-equilibrium) response based on the short-term response (Mansfield et al., 2020), in order to provide fast estimates of long-term response to different emissions perturbations.



480

Figure 6. Predicted temperature response for a 2050 time slice of emissions given by two SSP scenarios, where top panel shows input values for all pollutants in this year, with SSP1 (1.9) in blue and SSP3 (7.0) in red. The left hand panel maps show



the projected response (the difference between temperature at 2050 and present-day) and the hatching indicates regions where
485 the response exceeds the 1σ level predicted by the emulator (i.e., the sign of the response exceeds the natural variability). The
right hand panels show the global mean response predicted by the emulator, including the 1σ uncertainty estimate, which is
also in agreement with the impulse-response emulator FAIR (Smith, Forster, et al., 2018).

6 Conclusions

490 We have presented a new application of a Gaussian process emulator that estimates the *global pattern of response* to a sudden
change in emissions based on a carefully designed set of training data from the HadGEM3 coupled climate model. This
emulator has the ability to predict the spatial pattern of responses, rather than just the global mean responses as previous studies
have done (e.g., Castruccio et al., 2014; Meinshausen et al., 2011; Smith, Forster, et al., 2018). It predicts the short-term
495 temperature response to a range of global and regional perturbations that include both long-lived greenhouse gases and short-
lived aerosol pollutants.

Testing of the emulator shows accurate performance across most of the input space. This makes it a useful tool for predictions
of scenarios with more realistic aerosol perturbations, which are more relevant to climate policy studies, since large increases
500 in SO_2 emissions are unlikely under most climate projection scenarios (Riahi et al., 2017).

The main source of uncertainty in the emulator predictions is the internal variability of the GCM. Since this is also a source of
uncertainty in GCM runs on the same timescales, the choice of simulating climate response with an emulator is a sensible one.
Naturally, one of the next steps would be to reduce this uncertainty, for example, simulations could be averaged over longer
505 timescales (e.g., 10 or 20 years) to reduce the effect of year-to-year fluctuations, although this would require a substantial
increase in runtime per simulation. Emulator prediction uncertainty could also be targeted by increasing the size of the training
dataset. In addition, we assumed here that the internal variability is constant under different scenarios. In future work, it would
be interesting to explore how well this assumption holds by estimating the internal variability for each training simulation
independently, for example, by performing an ensemble of simulations each seeded with different initial conditions, for all 80
510 training simulations. Another extension of this work could involve building an additional GP emulator that explicitly models
the internal variability (heteroscedasticity, e.g., Gramacy, 2020).

We have demonstrated an example of how the emulator could be used to estimate the fast response (adjustment) to a sudden
perturbation in emissions, which may be of interest in policy-related analyses, by taking a timeslice of mid-century projected
515 emissions under two different SSP scenarios. These projections demonstrate how the emulator can be used to predict the spatial
response of surface temperature to a specific scenario featuring emission changes from different pollutants at a fraction of the
cost of the complete GCM. Running a GCM under this setting for five years would take on the order of days to estimate the



climate response, whereas the emulator prediction takes on the order of seconds. This type of tool could benefit policy studies in widening the number of scenarios that could be explored in a limited period of time.

520

We also identify the opportunity of coupling this fast adjustment emulator with a long-term response emulator, such as that presented in Mansfield et al. (2020), which could lead to full long-term climate projections. Similarly, we see scope to extend on our work by generating similar emulators from the output of other GCMs, for example to characterize inter-model uncertainty in the relationships derived here. Finally, additional forcings, such as those from separate biomass burning aerosol components, ozone precursors and/or natural aerosols, could also be included in such an emulator. We thus highlight Gaussian process emulators as a useful method to accelerate and understand regional climate change projections under varying anthropogenic emissions scenarios, including not only responses to GHG forcings but also, importantly, to short-lived forcing agents such as aerosols.

525

530 **Acknowledgments**

There are no financial conflicts of interests for any author. LAM was funded through EPSRC grant EP/L016613/1. PJN was supported through an Imperial College Research Fellowship and UK Natural Environment Research Council (NERC) grant number NE/V012045/1. AV is partially funded by the Leverhulme Trust, grant RC-2018-023, AXA Research Fund (project ‘AXA Chair in Wildfires and Climate’) and by the Hellenic Foundation for Research and Innovation (Grant ID 3453). EMR and OW were partly supported through NERC grant NE/N003411/1. Simulations with HadGEM3 were performed using the MONSooN system, a collaborative facility supplied under the Joint Weather and Climate Research Programme, which is a strategic partnership between the Met Office and the Natural Environment Research Council. Analysis was carried out on Imperial College London’s high performance computing cluster.

535

540 **Code and Data Availability**

Data was produced using HadGEM3, developed by the UK Met Office. Code and data used to train the emulator and produce all plots for this manuscript are available at <https://doi.org/10.5281/zenodo.17814594> (Mansfield, 2025)

Author Contribution

545 Conceptualisation: AV, PJN, LAM. Supervision: AV, PJN. Formal analysis: LAM, PJN, AV. Software: LAM, Validation: LAM, PJN, EMR, OW, AV. Methodology: LAM, PJN, EMR, OW, AV. Writing (original draft): LAM. Writing (review and editing): LAM, PJN, EMR, OW, AV.

Competing Interests

550 The authors declare that they have no conflicts of interest.



References

- Aamaas, B., Berntsen, T. K., Fuglestad, J. S., Shine, K. P., & Collins, W. J. (2017). Regional temperature change potentials for short-lived climate forcers based on radiative forcing from multiple models. *Atmospheric Chemistry and Physics*, 17(17), 10795–10809. <https://doi.org/10.5194/acp-17-10795-2017>
- Aamaas, B., Berntsen, T. K., & Samset, B. H. (2019). The regional temperature implications of strong air quality measures. *Atmospheric Chemistry and Physics*, 19(24), 15235–15245. <https://doi.org/10.5194/acp-19-15235-2019>
- Andrews, M. B., Ridley, J. K., Wood, R. A., Andrews, T., Blockley, E. W., Booth, B., Burke, E., Dittus, A. J., Florek, P., Gray, L. J., Haddad, S., Hardiman, S. C., Hermanson, L., Hodson, D., Hogan, E., Jones, G. S., Knight, J. R., Kuhlbrodt, T., Misios, S., ... Sutton, R. T. (2020). Historical Simulations With HadGEM3-GC3.1 for CMIP6. *Journal of Advances in Modeling Earth Systems*. <https://doi.org/10.1029/2019MS001995>
- Baker, L. H., Collins, W. J., Olivie, D. J. L., Cherian, R., Hodnebrog, Ø., Myhre, G., & Quaas, J. (2015). Climate responses to anthropogenic emissions of short-lived climate pollutants. *Atmospheric Chemistry and Physics*, 15(14), 8201–8216. <https://doi.org/10.5194/acp-15-8201-2015>
- Baker, L. H., Collins, W. J., Olivie, D. J. L., Cherian, R., Hodnebrog, Ø., Myhre, G., Quaas, J., & Samset, B. H. (2015). *Climate responses to anthropogenic emissions of short-lived climate pollutants* [Preprint]. Aerosols/Atmospheric Modelling/Troposphere/Physics (physical properties and processes). <https://doi.org/10.5194/acpd-15-3823-2015>
- Bao, J., McInerney, D. J., & Stein, M. L. (2016). A spatial-dependent model for climate emulation. *Environmetrics*, 27(7), 396–408. <https://doi.org/10.1002/env.2412>
- Beddows, A. V., Kitwiroon, N., Williams, M. L., & Beevers, S. D. (2017). Emulation and Sensitivity Analysis of the Community Multiscale Air Quality Model for a UK Ozone Pollution Episode. *Environmental Science and Technology*. <https://doi.org/10.1021/acs.est.6b05873>
- Beusch, L., Nicholls, Z., Gudmundsson, L., Hauser, M., Meinshausen, M., & Seneviratne, S. I. (2022). From emission scenarios to spatially resolved projections with a chain of computationally efficient emulators: Coupling of MAGICC (v7.5.1) and MESMER (v0.8.3). *Geoscientific Model Development*, 15(5), 2085–2103. <https://doi.org/10.5194/gmd-15-2085-2022>
- Boer, G. J., & Yu, B. (2003). Climate sensitivity and response. *Climate Dynamics*. <https://doi.org/10.1007/s00382-002-0283-3>
- Bolton, T., & Zanna, L. (2019). Applications of Deep Learning to Ocean Data Inference and Subgrid Parameterization. *Journal of Advances in Modeling Earth Systems*. <https://doi.org/10.1029/2018MS001472>
- Boucher, O., Granier, C., Hoose, C., & Jones, A. (2013). IPCC 2013 Chapter 7—Clouds and aerosols. *Climate Change 2013 the Physical Science Basis: Working Group I Contribution to the Fifth Assessment Report of the Intergovernmental Panel on Climate Change*.
- Bounceur, N., Crucifix, M., & Wilkinson, R. D. (2015). Global sensitivity analysis of the climate-vegetation system to astronomical forcing: An emulator-based approach. *Earth System Dynamics*. <https://doi.org/10.5194/esd-6-205-2015>
- Boussard, J., Nagda, C., Kaltenborn, J., Lange, C. E. E., Brouillard, P., Gurwicz, Y., Nowack, P., & Rolnick, D. (2023). *Towards Causal Representations of Climate Model Data* (arXiv:2312.02858). arXiv. <https://doi.org/10.48550/arXiv.2312.02858>
- Cachay, S. R., Henn, B., Watt-Meyer, O., Bretherton, C. S., & Yu, R. (2024). *Probabilistic Emulation of a Global Climate Model with Spherical DYffusion* (arXiv:2406.14798). arXiv. <https://doi.org/10.48550/arXiv.2406.14798>
- Cachier, H., Brémond, M. P., & Buat-Ménard, P. (1989). Carbonaceous aerosols from different tropical biomass burning sources. *Nature*. <https://doi.org/10.1038/340371a0>
- Carslaw, K. S., Lee, L. A., Reddington, C. L., Mann, G. W., & Pringle, K. J. (2013). The magnitude and sources of uncertainty in global aerosol. *Faraday Discussions*. <https://doi.org/10.1039/c3fd00043e>
- Carslaw, K. S., Lee, L. A., Reddington, C. L., Pringle, K. J., Rap, A., Forster, P. M., Mann, G. W., Spracklen, D. V., Woodhouse, M. T., Regayre, L. A., & Pierce, J. R. (2013). Large contribution of natural aerosols to uncertainty in indirect forcing. *Nature*. <https://doi.org/10.1038/nature12674>



- 600 Castruccio, S., McInerney, D. J., Stein, M. L., Liu Crouch, F., Jacob, R. L., & Moyer, E. J. (2014). Statistical Emulation of
 Climate Model Projections Based on Precomputed GCM Runs. *Journal of Climate*, 27(5), 1829–1844.
<https://doi.org/10.1175/JCLI-D-13-00099.1>
- Collins, W. J., Fry, M. M., Yu, H., Fuglestedt, J. S., Shindell, D. T., & West, J. J. (2013). Global and regional temperature-
 change potentials for near-term climate forcings. *Atmospheric Chemistry and Physics*. [https://doi.org/10.5194/acp-](https://doi.org/10.5194/acp-13-2471-2013)
 605 13-2471-2013
- Corti, S., Molteni, F., & Palmer, T. N. (1999). Signature of recent climate change in frequencies of natural atmospheric
 circulation regimes. *Nature*. <https://doi.org/10.1038/19745>
- Curran, C., Mitchell, T., Morris, M., & Ylvisaker, D. (1991). Bayesian prediction of deterministic functions, with
 applications to the design and analysis of computer experiments. *Journal of the American Statistical Association*.
 610 <https://doi.org/10.1080/01621459.1991.10475138>
- Dong, B., Sutton, R. T., Highwood, E., & Wilcox, L. (2014). The impacts of European and Asian anthropogenic sulfur
 dioxide emissions on Sahel rainfall. *Journal of Climate*. <https://doi.org/10.1175/JCLI-D-13-00769.1>
- Durack, P. J., Naik, V., Nicholls, Z., O'Rourke, E., Turner, B., Buontempo, C., Brookshaw, A., Goddard, C., MacIntosh, C.,
 Hewitt, H., & Dunne, J. (2025). Earth System Forcing for CMIP7 and Beyond. *Bulletin of the American*
 615 *Meteorological Society*, 106(8), E1580–E1588. <https://doi.org/10.1175/BAMS-D-25-0119.1>
- ECLIPSE. (2014). *ECLIPSE V5 global emission fields*. International Institute for Applied Systems Analysis.
- Edwards, T. L., Brandon, M. A., Durand, G., Edwards, N. R., Golledge, N. R., Holden, P. B., Nias, I. J., Payne, A. J., Ritz,
 C., & Wernecke, A. (2019). Revisiting Antarctic ice loss due to marine ice-cliff instability. *Nature*.
<https://doi.org/10.1038/s41586-019-0901-4>
- 620 Foley, A. M., Holden, P. B., Edwards, N. R., Mercure, J. F., Salas, P., Pollitt, H., & Chewpreecha, U. (2016). Climate model
 emulation in an integrated assessment framework: A case study for mitigation policies in the electricity sector.
Earth System Dynamics. <https://doi.org/10.5194/esd-7-119-2016>
- Forster, P., Storelvmo, T., Armour, K., Collins, W., Dufresne, J.-L., Frame, D., Lunt, D. J., Mauritsen, T., Palmer, M. D.,
 Watanabe, M., Wild, M., & Zhang, H. (2021). The Earth's Energy Budget, Climate Feedbacks, and Climate
 625 Sensitivity. In V. Masson-Delmotte, P. Zhai, A. Pirani, S. L. Connors, C. Péan, S. Berger, N. Caud, Y. Chen, L.
 Goldfarb, M. I. Gomis, M. Huang, K. Leitzell, E. Lonnoy, J. B. R. Matthews, T. K. Maycock, T. Waterfield, O.
 Yelekçi, R. Yu, & B. Zhou (Eds.), *Climate Change 2021: The Physical Science Basis. Contribution of Working*
Group I to the Sixth Assessment Report of the Intergovernmental Panel on Climate Change (pp. 923–1054).
 Cambridge University Press. <https://doi.org/10.1017/9781009157896.009>
- 630 Gidden, M. J., Riahi, K., Smith, S. J., Fujimori, S., Luderer, G., Kriegler, E., Van Vuuren, D. P., Van Den Berg, M., Feng,
 L., Klein, D., Calvin, K., Doelman, J. C., Frank, S., Fricko, O., Harmsen, M., Hasegawa, T., Havlik, P., Hilaire, J.,
 Hoesly, R., ... Takahashi, K. (2019). Global emissions pathways under different socioeconomic scenarios for use in
 CMIP6: A dataset of harmonized emissions trajectories through the end of the century. *Geoscientific Model*
Development. <https://doi.org/10.5194/gmd-12-1443-2019>
- 635 GPy. (2012). *GPy: A Gaussian process framework in python*. <http://github.com/SheffieldML/GPy>
- Gramacy, R. B. (2020). *Surrogates: Gaussian Process Modeling, Design and Optimization for the Applied Sciences*.
 Chapman Hall/CRC.
- Gregory, J. M., Ingram, W. J., Palmer, M. A., Jones, G. S., Stott, P. A., Thorpe, R. B., Lowe, J. A., Johns, T. C., & Williams,
 K. D. (2004). A new method for diagnosing radiative forcing and climate sensitivity. *Geophysical Research Letters*,
 640 31(3). <https://doi.org/10.1029/2003GL018747>
- Guan, H., Arcomano, T., Chattopadhyay, A., & Maulik, R. (2024). *LUCIE: A Lightweight Uncoupled Climate Emulator*
with long-term stability and physical consistency for O(1000)-member ensembles (arXiv:2405.16297). arXiv.
<https://doi.org/10.48550/arXiv.2405.16297>
- Hansen, J., Sato, M., & Ruedy, R. (1997). Radiative forcing and climate response. *Journal of Geophysical Research*
 645 *Atmospheres*. <https://doi.org/10.1029/96JD03436>
- Hansen, J., Sato, M., Ruedy, R., Nazarenko, L., Lacis, A., Schmidt, G. A., Russell, G., Aleinov, I., Bauer, M., Bauer, S.,
 Bell, N., Cairns, B., Canuto, V., Chandler, M., Cheng, Y., Del Genio, A., Faluvegi, G., Fleming, E., Friend, A., ...
 Zhang, S. (2005). Efficacy of climate forcings. In *Journal of Geophysical Research D: Atmospheres* (Vol. 110,
 Issue 18, pp. 1–45). <https://doi.org/10.1029/2005JD005776>



- 650 Haywood, J., & Boucher, O. (2000). Estimates of the direct and indirect radiative forcing due to tropospheric aerosols: A review. In *Reviews of Geophysics*. <https://doi.org/10.1029/1999RG000078>
- Hodnebrog, O., Myhre, G., Forster, P. M., Sillmann, J., & Samset, B. H. (2016). Local biomass burning is a dominant cause of the observed precipitation reduction in southern Africa. *Nature Communications*. <https://doi.org/10.1038/ncomms11236>
- 655 Joshi, M., Shine, K., Ponater, M., Stuber, N., Sausen, R., & Li, L. (2003). A comparison of climate response to different radiative forcings in three general circulation models: Towards an improved metric of climate change. *Climate Dynamics*, 20(7), 843–854. <https://doi.org/10.1007/s00382-003-0305-9>
- Kaltenborn, J., Lange, C. E. E., Ramesh, V., Brouillard, P., Gurwicz, Y., Nagda, C., Runge, J., Nowack, P., & Rolnick, D. (2023). *ClimateSet: A Large-Scale Climate Model Dataset for Machine Learning* (arXiv:2311.03721). arXiv. <http://arxiv.org/abs/2311.03721>
- 660 Kasoar, M., Shawki, D., & Voulgarakis, A. (2018). Similar spatial patterns of global climate response to aerosols from different regions. *Npj Climate and Atmospheric Science*, 1(1), 12. <https://doi.org/10.1038/s41612-018-0022-z>
- King, R. C., Mansfield, L. A., & Sheshadri, A. (2024). Bayesian History Matching Applied to the Calibration of a Gravity Wave Parameterization. *Journal of Advances in Modeling Earth Systems*, 16(4), e2023MS004163. <https://doi.org/10.1029/2023MS004163>
- 665 Lasslop, G., Coppola, A. I., Voulgarakis, A., Yue, C., & Veraverbeke, S. (2019). Influence of Fire on the Carbon Cycle and Climate. In *Current Climate Change Reports*. <https://doi.org/10.1007/s40641-019-00128-9>
- Lee, L. A., Carslaw, K. S., Pringle, K. J., & Mann, G. W. (2012). Mapping the uncertainty in global CCN using emulation. *Atmospheric Chemistry and Physics*. <https://doi.org/10.5194/acp-12-9739-2012>
- 670 Lee, L. A., Carslaw, K. S., Pringle, K. J., Mann, G. W., & Spracklen, D. V. (2011). Emulation of a complex global aerosol model to quantify sensitivity to uncertain parameters. *Atmospheric Chemistry and Physics*. <https://doi.org/10.5194/acp-11-12253-2011>
- Lee, L. A., Reddington, C. L., & Carslaw, K. S. (2016). On the relationship between aerosol model uncertainty and radiative forcing uncertainty. *Proceedings of the National Academy of Sciences of the United States of America*. <https://doi.org/10.1073/pnas.1507050113>
- 675 Lewinschal, A., Ekman, A. M. L., Hansson, H. C., Sand, M., Berntsen, T. K., & Langner, J. (2019). Local and remote temperature response of regional SO₂ emissions. *Atmospheric Chemistry and Physics*. <https://doi.org/10.5194/acp-19-2385-2019>
- Lioussse, C., Assamoi, E., Criqui, P., Granier, C., & Rosset, R. (2014). Explosive growth in African combustion emissions from 2005 to 2030. *Environmental Research Letters*. <https://doi.org/10.1088/1748-9326/9/3/035003>
- 680 Loepky, J. L., Sacks, J., & Welch, W. J. (2009). Choosing the sample size of a computer experiment: A practical guide. *Technometrics*. <https://doi.org/10.1198/TECH.2009.08040>
- Mann, G. W., Carslaw, K. S., Spracklen, D. V., Ridley, D. A., Manktelow, P. T., Chipperfield, M. P., Pickering, S. J., & Johnson, C. E. (2010). Description and evaluation of GLOMAP-mode: A modal global aerosol microphysics model for the UKCA composition-climate model. *Geoscientific Model Development*. <https://doi.org/10.5194/gmd-3-519-2010>
- 685 Mansfield, L. A. (2025). *Lm2612/emulator* (Version First release (v1.0)) [Computer software]. Zenodo. <https://doi.org/10.5281/zenodo.17814595>
- Mansfield, L. A., Nowack, P. J., Kasoar, M., Everitt, R. G., Collins, W. J., & Voulgarakis, A. (2020). Predicting global patterns of long-term climate change from short-term simulations using machine learning. *Npj Climate and Atmospheric Science*. <https://doi.org/10.1038/s41612-020-00148-5>
- 690 Meinshausen, M., Nicholls, Z. R. J., Lewis, J., Gidden, M. J., Vogel, E., Freund, M., Beyerle, U., Gessner, C., Nauels, A., Bauer, N., Canadell, J. G., Daniel, J. S., John, A., Krummel, P. B., Luderer, G., Meinshausen, N., Montzka, S. A., Rayner, P. J., Reimann, S., ... Wang, R. H. J. (2020). The shared socio-economic pathway (SSP) greenhouse gas concentrations and their extensions to 2500. *Geoscientific Model Development*, 13(8), 3571–3605. <https://doi.org/10.5194/gmd-13-3571-2020>
- 695 Meinshausen, M., Raper, S. C. B., & Wigley, T. M. L. (2011). Emulating coupled atmosphere-ocean and carbon cycle models with a simpler model, MAGICC6 – Part 1: Model description and calibration. *Atmospheric Chemistry and Physics*, 11(4), 1417–1456. <https://doi.org/10.5194/acp-11-1417-2011>



- 700 Met Office. (2021). The Cray XC40 supercomputing system. *https://www.metoffice.gov.uk/about-us/what/technology/supercomputer*. Date Accessed: 21/06/2021.
- Nath, S., Lejeune, Q., Beusch, L., Seneviratne, S. I., & Schleussner, C.-F. (2022). MESMER-M: an Earth system model emulator for spatially resolved monthly temperature. *Earth System Dynamics*, 13(2), 851–877. <https://doi.org/10.5194/esd-13-851-2022>
- 705 Nicholls, Z. R. J., Meinshausen, M., Lewis, J., Gieseke, R., Dommenges, D., Dorheim, K., Fan, C.-S., Fuglestad, J. S., Gasser, T., Golüke, U., Goodwin, P., Hartin, C., Hope, A. P., Kriegl, E., Leach, N. J., Marchegiani, D., McBride, L. A., Quilcaille, Y., Rogelj, J., ... Xie, Z. (2020). Reduced Complexity Model Intercomparison Project Phase 1: Introduction and evaluation of global-mean temperature response. *Geoscientific Model Development*, 13(11), 5175–5190. <https://doi.org/10.5194/gmd-13-5175-2020>
- 710 Nowack, P., Braesicke, P., Haigh, J., Abraham, N. L., Pyle, J., & Voulgarakis, A. (2018). Using machine learning to build temperature-based ozone parameterizations for climate sensitivity simulations. *Environmental Research Letters*. <https://doi.org/10.1088/1748-9326/aae2be>
- O’Hagan, A. (1978). Curve Fitting and Optimal Design for Prediction. *Journal of the Royal Statistical Society: Series B (Methodological)*. <https://doi.org/10.1111/j.2517-6161.1978.tb01643.x>
- 715 Palmer, T. N. (1999). A nonlinear dynamical perspective on climate prediction. *Journal of Climate*. [https://doi.org/10.1175/1520-0442\(1999\)012<0575:ANDPOC>2.0.CO;2](https://doi.org/10.1175/1520-0442(1999)012<0575:ANDPOC>2.0.CO;2)
- Pechony, O., & Shindell, D. T. (2010). Driving forces of global wildfires over the past millennium and the forthcoming century. *Proceedings of the National Academy of Sciences of the United States of America*. <https://doi.org/10.1073/pnas.1003669107>
- 720 Persad, G. G., & Caldeira, K. (2018). Divergent global-scale temperature effects from identical aerosols emitted in different regions. *Nature Communications*, 9(1), Article 1. <https://doi.org/10.1038/s41467-018-05838-6>
- Popp, A., Calvin, K., Fujimori, S., Havlik, P., Humpenöder, F., Stehfest, E., Bodirsky, B. L., Dietrich, J. P., Doelmann, J. C., Gusti, M., Hasegawa, T., Kyle, P., Obersteiner, M., Tabeau, A., Takahashi, K., Valin, H., Waldhoff, S., Weindl, I., Wise, M., ... Vuuren, D. P. van. (2017). Land-use futures in the shared socio-economic pathways. *Global Environmental Change*. <https://doi.org/10.1016/j.gloenvcha.2016.10.002>
- 725 Rasmussen, C. E., & Williams, C. K. I. (2006). *Gaussian processes for machine learning*. MIT Press.
- Rasp, S., Pritchard, M. S., & Gentile, P. (2018). Deep learning to represent subgrid processes in climate models. *Proceedings of the National Academy of Sciences of the United States of America*. <https://doi.org/10.1073/pnas.1810286115>
- 730 Riahi, K., van Vuuren, D. P., Kriegler, E., Edmonds, J., O’Neill, B. C., Fujimori, S., Bauer, N., Calvin, K., Dellink, R., Fricko, O., Lutz, W., Popp, A., Cuaserna, J. C., KC, S., Leimbach, M., Jiang, L., Kram, T., Rao, S., Emmerling, J., ... Tavoni, M. (2017). The Shared Socioeconomic Pathways and their energy, land use, and greenhouse gas emissions implications: An overview. *Global Environmental Change*. <https://doi.org/10.1016/j.gloenvcha.2016.05.009>
- 735 Richardson, T. B., Forster, P. M., Smith, C. J., Maycock, A. C., Wood, T., Andrews, T., Boucher, O., Faluvegi, G., Fläschner, D., Hodnebrog, K., Kasoari, M., Kirkevåg, A., Lamarque, J. F., Mülmenstädt, J., Myhre, G., Olivé, D., Portmann, R. W., Samset, B. H., Shawki, D., ... Watson-Parris, D. (2019). Efficacy of Climate Forcings in PDRMIP Models. *Journal of Geophysical Research: Atmospheres*. <https://doi.org/10.1029/2019JD030581>
- 740 Ridley, J. K., Blockley, E. W., Keen, A. B., Rae, J. G. L., West, A. E., & Schroeder, D. (2018). The sea ice model component of HadGEM3-GC3.1. *Geoscientific Model Development*, 11(2), 713–723. <https://doi.org/10.5194/gmd-11-713-2018>
- Ring, M. J., & Plumb, R. A. (2008). The response of a simplified GCM to axisymmetric forcings: Applicability of the fluctuation-dissipation theorem. *Journal of the Atmospheric Sciences*. <https://doi.org/10.1175/2008JAS2773.1>
- Ryan, E., Wild, O., Voulgarakis, A., & Lee, L. (2018). Fast sensitivity analysis methods for computationally expensive models with multi-dimensional output. *Geoscientific Model Development*, 11, 3131–3146. <https://doi.org/10.5194/gmd-11-3131-2018>
- 745 Saltelli, A., Aleksankina, K., Becker, W., Fennell, P., Ferretti, F., Holst, N., Li, S., & Wu, Q. (2019). Why so many published sensitivity analyses are false: A systematic review of sensitivity analysis practices. *Environmental Modelling and Software*. <https://doi.org/10.1016/j.envsoft.2019.01.012>



- 750 Saltelli, A., & Annoni, P. (2010). How to avoid a perfunctory sensitivity analysis. *Environmental Modelling and Software*.
<https://doi.org/10.1016/j.envsoft.2010.04.012>
- Saltelli, A., Annoni, P., Azzini, I., Campolongo, F., Ratto, M., & Tarantola, S. (2010). Variance based sensitivity analysis of model output. Design and estimator for the total sensitivity index. *Computer Physics Communications*.
<https://doi.org/10.1016/j.cpc.2009.09.018>
- 755 Saltelli, A., Ratto, M., Andres, T., Campolongo, F., Cariboni, J., Gatelli, D., Saisana, M., & Tarantola, S. (2008). Global Sensitivity Analysis. The Primer. In *Global Sensitivity Analysis. The Primer*.
<https://doi.org/10.1002/9780470725184>
- Salter, J. M., & Williamson, D. (2016). A comparison of statistical emulation methodologies for multi-wave calibration of environmental models. *Environmetrics*. <https://doi.org/10.1002/env.2405>
- 760 Samset, B. H., Sand, M., Smith, C. J., Bauer, S. E., Forster, P. M., Fuglestedt, J. S., Osprey, S., & Schleussner, C.-F. (2018). Climate Impacts From a Removal of Anthropogenic Aerosol Emissions. *Geophysical Research Letters*, 45(2), 1020–1029.
- Santner, T. J., Williams, B. J., Notz, W. I., & Williams, B. J. (2003). *The design and analysis of computer experiments* (Vol. 1). Springer.
- 765 Shawki, D., Voulgarakis, A., Chakraborty, A., Kassoar, M., & Srinivasan, J. (2018). The South Asian Monsoon Response to Remote Aerosols: Global and Regional Mechanisms. *Journal of Geophysical Research: Atmospheres*.
<https://doi.org/10.1029/2018JD028623>
- Shindell, D., & Faluvegi, G. (2009). Climate response to regional radiative forcing during the twentieth century. *Nature Geoscience*, 2, 294 EP-. <https://doi.org/10.1038/ngeo473>
- 770 Shindell, D. T. (2012). Evaluation of the absolute regional temperature potential. *Atmospheric Chemistry and Physics*, 12(17), 7955–7960. <https://doi.org/10.5194/acp-12-7955-2012>
- Shindell, D. T., Miller, R. L., Schmidt, G. A., & Pandolfo, L. (1999). Simulation of recent northern winter climate trends by greenhouse-gas forcing. *Nature*. <https://doi.org/10.1038/20905>
- Smith, C. J., Forster, P. M., Allen, M., Leach, N., Millar, R. J., Passerello, G. A., & Regayre, L. A. (2018). FAIR v1.3: A simple emissions-based impulse response and carbon cycle model. *Geoscientific Model Development*.
<https://doi.org/10.5194/gmd-11-2273-2018>
- 775 Smith, C. J., Kramer, R. J., Myhre, G., Forster, P. M., Soden, B. J., Andrews, T., Boucher, O., Faluvegi, G., Fläschner, D., Hodnebrog, Ø., Kassoar, M., Kharin, V., Kirkevåg, A., Lamarque, J.-F., Mülmenstädt, J., Olivé, D., Richardson, T., Samset, B. H., Shindell, D., ... Watson-Parris, D. (2018). Understanding Rapid Adjustments to Diverse Forcing Agents. *Geophysical Research Letters*, 45(21), 12,023–12,031. <https://doi.org/10.1029/2018GL079826>
- 780 Souza, A. N., Wagner, G. L., Ramadhan, A., Allen, B., Churavy, V., Schloss, J., Campin, J., Hill, C., Edelman, A., Marshall, J., Flierl, G., & Ferrari, R. (2020). Uncertainty Quantification of Ocean Parameterizations: Application to the K-Profile-Parameterization for Penetrative Convection. *Journal of Advances in Modeling Earth Systems*.
<https://doi.org/10.1029/2020MS002108>
- 785 Stell, A. C., Western, L. M., Sherwen, T., & Rigby, M. (2021). Atmospheric-methane source and sink sensitivity analysis using Gaussian process emulation. *Atmospheric Chemistry and Physics*. <https://doi.org/10.5194/acp-21-1717-2021>
- Stocker, T. (2013). IPCC Summary for Policymakers in Climate Change 2013: The Physical Science Basis. In *Climate Change Lecture Series*.
- Stohl, A., Aamaas, B., Amann, M., Baker, L. H., Bellouin, N., Bernsten, T. K., Boucher, O., Cherian, R., Collins, W., Daskalakis, N., Dusinska, M., Eckhardt, S., Fuglestedt, J. S., Harju, M., Heyes, C., Hodnebrog, Ø., Hao, J., Im, U., Kanakidou, M., ... Zhu, T. (2015). Evaluating the climate and air quality impacts of short-lived pollutants. *Atmospheric Chemistry and Physics*, 15(18), 10529–10566. <https://doi.org/10.5194/acp-15-10529-2015>
- 790 Storkey, D., Blaker, A. T., Mathiot, P., Megann, A., Aksenov, Y., Blockley, E. W., Calvert, D., Graham, T., Hewitt, H. T., Hyder, P., Kuhlbrodt, T., Rae, J. G. L., & Sinha, B. (2018). UK Global Ocean GO6 and GO7: A traceable hierarchy of model resolutions. *Geoscientific Model Development*, 11(8), 3187–3213. <https://doi.org/10.5194/gmd-11-3187-2018>
- 795 Tosca, M. G., Randerson, J. T., & Zender, C. S. (2013). Global impact of smoke aerosols from landscape fires on climate and the Hadley circulation. *Atmospheric Chemistry and Physics*. <https://doi.org/10.5194/acp-13-5227-2013>



- Urrego-Blanco, J. R., Urban, N. M., Hunke, E. C., Turner, A. K., & Jeffery, N. (2016). Uncertainty quantification and global
 800 sensitivity analysis of the Los Alamos sea ice model. *Journal of Geophysical Research: Oceans*.
<https://doi.org/10.1002/2015JC011558>
- Van der Werf, G. R., Randerson, J. T., Collatz, G. J., & Giglio, L. (2003). Carbon emissions from fires in tropical and
 subtropical ecosystems. *Global Change Biology*. <https://doi.org/10.1046/j.1365-2486.2003.00604.x>
- van Vuuren, D. P., Stehfest, E., Gernaat, D. E. H. J., Doelman, J. C., van den Berg, M., Harmsen, M., de Boer, H. S.,
 805 Bouwman, L. F., Daioglou, V., Edelenbosch, O. Y., Girod, B., Kram, T., Lassaletta, L., Lucas, P. L., van Meijl, H.,
 Müller, C., van Ruijven, B. J., van der Sluis, S., & Tabeau, A. (2017). Energy, land-use and greenhouse gas
 emissions trajectories under a green growth paradigm. *Global Environmental Change*.
<https://doi.org/10.1016/j.gloenvcha.2016.05.008>
- Voulgarakis, A., & Field, R. D. (2015). Fire Influences on Atmospheric Composition, Air Quality and Climate. In *Current
 810 Pollution Reports*. <https://doi.org/10.1007/s40726-015-0007-z>
- Walters, D., Baran, A. J., Boutle, I., Brooks, M., Earnshaw, P., Edwards, J., Furtado, K., Hill, P., Lock, A., Manners, J.,
 Morcrette, C., Mulcahy, J., Sanchez, C., Smith, C., Stratton, R., Tennant, W., Tomassini, L., Van Weverberg, K.,
 Vosper, S., ... Zerroukat, M. (2019). The Met Office Unified Model Global Atmosphere 7.0/7.1 and JULES Global
 Land 7.0 configurations. *Geoscientific Model Development*, 12(5), 1909–1963. <https://doi.org/10.5194/gmd-12-1909-2019>
- 815 Ward, D. S., Kloster, S., Mahowald, N. M., Rogers, B. M., Randerson, J. T., & Hess, P. G. (2012). The changing radiative
 forcing of fires: Global model estimates for past, present and future. *Atmospheric Chemistry and Physics*.
<https://doi.org/10.5194/acp-12-10857-2012>
- Watson-Parris, D. (2021). Machine learning for weather and climate are worlds apart. In *Philosophical Transactions of the
 820 Royal Society A: Mathematical, Physical and Engineering Sciences*. <https://doi.org/10.1098/rsta.2020.0098>
- Watt-Meyer, O., Dresdner, G., McGibbon, J., Clark, S. K., Henn, B., Duncan, J., Brenowitz, N. D., Kashinath, K., Pritchard,
 M. S., Bonev, B., Peters, M. E., & Bretherton, C. S. (2023). *ACE: A fast, skillful learned global atmospheric model
 for climate prediction* (arXiv:2310.02074). arXiv. <http://arxiv.org/abs/2310.02074>
- Watt-Meyer, O., Henn, B., McGibbon, J., Clark, S. K., Kwa, A., Perkins, W. A., Wu, E., Harris, L., & Bretherton, C. S.
 825 (2025). ACE2: Accurately learning subseasonal to decadal atmospheric variability and forced responses. *Npj
 Climate and Atmospheric Science*, 8(1), 205. <https://doi.org/10.1038/s41612-025-01090-0>
- Westervelt, D. M., Mascioli, N. R., Fiore, A. M., Conley, A. J., Lamarque, J. F., Shindell, D. T., Faluvegi, G., Previdi, M.,
 Correa, G., & Horowitz, L. W. (2020). Local and remote mean and extreme temperature response to regional
 aerosol emissions reductions. *Atmospheric Chemistry and Physics*. <https://doi.org/10.5194/acp-20-3009-2020>
- 830 Wild, O., Voulgarakis, A., O'Connor, F., Lamarque, J. F., Ryan, E. M., & Lee, L. (2020). Global sensitivity analysis of
 chemistry-climate model budgets of tropospheric ozone and OH: Exploring model diversity. *Atmospheric
 Chemistry and Physics*. <https://doi.org/10.5194/acp-20-4047-2020>
- Williams, K. D., Copsey, D., Blockley, E. W., Bodas-Salcedo, A., Calvert, D., Comer, R., Davis, P., Graham, T., Hewitt, H.
 T., Hill, R., Hyder, P., Ineson, S., Johns, T. C., Keen, A. B., Lee, R. W., Megann, A., Milton, S. F., Rae, J. G. L.,
 835 Roberts, M. J., ... Xavier, P. K. (2018). The Met Office Global Coupled Model 3.0 and 3.1 (GC3.0 and GC3.1)
 Configurations. *Journal of Advances in Modeling Earth Systems*, 10(2), 357–380.
<https://doi.org/10.1002/2017MS001115>
- Williamson, D., Blaker, A. T., Hampton, C., & Salter, J. (2015). Identifying and removing structural biases in climate
 models with history matching. *Climate Dynamics*. <https://doi.org/10.1007/s00382-014-2378-z>

840